

Single Evoked Somatosensory MEG Responses Extracted by Time Delayed Decorrelation

Tilmann H. Sander, Martin Burghoff, Gabriel Curio, and Lutz Trahms

Abstract—Measurable magnetoencephalographic responses of the cortex due to an electrical stimulus at the wrist start 20 ms after the stimulus. This early magnetic response is known as the N20m, which can be seen by averaging over hundreds of stimulation epochs. Applying Independent Component Analysis (ICA) based on time-delayed decorrelation to such data allows the extraction of the single responses starting 20 ms after the stimulus without the need for averaging. One of the independent components has a field pattern that is very similar to the N20m. Using this independent component, it is found that the response at 20 ms is stable over a measurement session lasting 4000 s and containing 12 000 stimulations, whereas later responses show highly significant changes over time. To suppress slower activity and noise in the data, a high pass of 55 Hz is applied to the data. One of the subsequently calculated independent components shows that the response at 20 ms is much clearer than before filtering. Analyzing the amplitude distribution of this response yields that 97% of the stimulations have a measurable response above base line level, whereas for conventional methods such as projection and notch filtering, only 91% of the responses are detectable. The high degree of measurable responses indicates the signal separation power of independent component analysis, and it supports the hypothesis that the early stages of sensory cortical processing can be described as a linear processing chain with small variability, at least from a macroscopic point of view.

Index Terms—Independent component analysis, magnetoencephalography, medianus stimulation, somatosensory evoked fields, temporal decorrelation.

I. INTRODUCTION

THE noninvasive study of brain functions on a millisecond-timescale is most easily done using Electroencephalography (EEG) or Magnetoencephalography (MEG). This time resolution is partially lost as evoked brain responses can be obscured by spontaneous brain activity, other physiological signals, and technical noise sources. Individual brain responses due to a single stimulus can generally not be isolated, and only an average over several tens to thousands of identical stimulations yields a picture of the brain response. Naturally, the average cannot show variations in timing and amplitude in the response to consecutive individual stimulations. The assessment of variations in timing and amplitude is of great importance for un-

derstanding brain function in more detail as there exist, even for early cortical responses, the competing models of i) linear input-output processing with minimal variability and of ii) temporally and spatially distributed and highly variable processing. To isolate single responses from a stream of unaveraged multichannel data, Independent Component Analysis (ICA) is frequently applied. ICA is a method that decomposes a multivariate dataset such as multichannel EEG or MEG measurements into a superposition of spatially stationary patterns with statistically independent amplitude functions [1].

The ICA model has proven to be of great importance in the analysis of biomedical data such as MEG, EEG [1], [2], or functional magnetic resonance imaging [3], [4]. In the case of EEG/MEG, the ICA requirement for spatial stationarity is fulfilled for some brain activations generating noninvasively detectable signals. Although the neural signals are propagating along axons and dendrites, there exist macroscopic processing centers such as the somatosensory cortex, which are functionally and anatomically well circumscribed. The assumption of statistical independence between a stimulated response from, e.g., the somatosensory cortex and an unrelated response from the visual cortex due to the subject perceiving his/her environment is a plausible one. The same assumptions hold for certain types of noise and unwanted signals such as, e.g., eye and cardiac activity [1] and spontaneous brain activity [5], [6].

Thus far, few works have applied ICA to electrophysiological measurements of the early and weak brain responses due to somatosensory stimulation. An example of these responses is the somatosensory evoked field (SEF), which is caused by an electrical stimulation at the wrist. A short electrical pulse delivered to the median nerve on one hand leads to a sequence of neuronal activations in the somatosensory cortex contralateral to the stimulated side. The earliest cortical response observable in the MEG due to this type of stimulation can be seen at 20 ms. This so-called N20m is a very stable response that is essentially independent of the state of alertness, and it can be measured even during sleep. It was described in [7] using a seven-channel gradiometer, and the average response has been thoroughly studied [8], [9]. Recently, contradictory results have appeared in the literature with respect to the variability of individual somatosensory responses at 20 ms: In [10], it is found that the response at 20 ms even changes sign on consecutive stimulations, whereas the data shown in [11] imply large variability with rare occurrences of an amplitude close to zero. To further investigate the response variability at 20 ms, in this work, ICA is applied to unfiltered and highpass filtered SEFs. The averaged response at 20 ms typically has a width of only a few milliseconds, suggesting that the main features

Manuscript received September 30, 2004; revised March 22, 2005. This work was supported by SFB 618-B4 and BMBF under Grant 01G00208 BNIC (Berlin Neuroimaging Centre). The associate editor coordinating the review of this manuscript and approving it for publication was Dr. Jan C. de Munck.

T. H. Sander, M. Burghoff, and L. Trahms are with the Physikalisch-Technische Bundesanstalt, 10587 Berlin, Germany (e-mail: tilmann.sander-thoemmes@ptb.de; martin.burghoff@ptb.de; lutz.trahms@ptb.de).

G. Curio is with the Neurophysics Group, Department of Neurology, Campus Benjamin Franklin, Charité, 12200 Berlin, Germany (e-mail: gabriel.curio@charite.de).

Digital Object Identifier 10.1109/TSP.2005.853156

of this response will not be altered by highpass filtering the signal with a cutoff of up to 100 Hz.

Among several available ICA algorithms, the time-delayed decorrelation (TDD, TDSEP, SOBI) [12]–[14] has been applied frequently to MEG data [6], [15]–[21]. Only three of those studies are an application of ICA to SEF raw data. The TDD-ICA components due to tactile stimuli on the thumb after a press button action are studied in [17] and [18], and the third [21] studies interhemispheric connectivity phenomena by applying TDD-ICA to data obtained from unilateral electrical medianus nerve stimulation. The encouraging agreement between anatomical and physiological knowledge and parameters derived from TDD components due to somatosensory stimulation is described in [22] for high-density EEG data similar to the MEG data presented here. In contrast to these earlier reports, we focus on the best possible extraction of the single trial response at 20 ms using time domain filtering as a preprocessing tool before the TDD-ICA is applied. Note that filtering as preprocessing is compatible with the ICA model [1].

As a first step, the TDD algorithm is applied to SEF measurements, and the TDD result is validated using secondary information such as the conventional average. Then, individual TDD time series that can be associated with the N20m and later responses are characterized using a visualization of each individual response (single trial plot). The stability of the response sequence in the course of the experiment is assessed using a simple statistical measure applied to subgroups of individual responses. Finally, single trial statistics are calculated for the set of responses at 20 ms extracted from a single TDD component, which was obtained from highpass filtered data. These single trial statistics are compared with the result using the more conventional projection method.

II. METHODS

A. Time-Delayed Decorrelation

The MEG signal in each sensor is a superposition of the signal from a number of brain and (external) noise sources with unknown time dependence and of unknown spatial origin. Assuming stationarity as it is required for applying ICA [1], the data can be written as a sum of n sources of the form $s_i(t)\mathbf{a}_i$, where \mathbf{a}_i is a time-independent field pattern related to the m -channel sensor system, and $s_i(t)$ describes the time dependence of the source. These sources are abstract objects in a m -dimensional signal space, and generally, they should not be regarded as cortical sources. The pattern \mathbf{a}_i can be visualized as a field map using the sensor locations. Combining the $s_i(t)$ into the vector $\mathbf{s}(t)$ and the \mathbf{a}_i into matrix \mathbf{A} , the vector $\mathbf{x}(t)$ of the measured MEG time traces $x_i(t)$ is given by

$$\mathbf{x}(t) = \mathbf{A}\mathbf{s}(t). \quad (1)$$

The source amplitudes $s_i(t)$ and their maps \mathbf{a}_i are generally unknown. ICA algorithms aim to calculate for the case of an identical number of sources and sensors, i.e., $m = n$, a demixing matrix \mathbf{W}^{-1} fulfilling

$$\mathbf{W}^{-1}\mathbf{x}(t) = \mathbf{u}(t) \quad (2)$$

where the $u_i(t)$ are identical to the $s_i(t)$ if disregarding an indeterminacy in scale and ordering. For clarity, note that the term “ICA component” means the function $\mathbf{w}_i u_i(t)$, where the base vector \mathbf{w}_i can be visualized as a field map. The demixing matrix can be used in two ways for further data processing: i) signal rejection by setting columns corresponding to unwanted signals in \mathbf{W} to zero and then applying the modified matrix to $\mathbf{u}(t)$ and ii) time domain signal analysis on selected one-dimensional (1-D) amplitude functions $u_i(t)$. The second case is pursued in this work.

For signals with characteristic spectra or even periodic signals with harmonic spectra, an ICA algorithm was suggested, exploiting the nonzero time-lagged cross-correlations between different measured channels. The TDD [12]–[14] algorithm is essentially an approximate simultaneous diagonalization of several delayed covariance matrices

$$C_{ij}(\tau_k) = \sum_l x_i(t_l)x_j(t_l + \tau_k) \quad (3)$$

for a fixed set of time delays τ_k . For computational efficiency, the diagonalization is performed on the set of whitened symmetrized delayed covariance matrices, where the whitening uses the covariance matrix (i.e., $\tau = 0$).

In [23], it was shown that the symmetrized delayed covariance matrices $C_{ij}^{sym}(\tau_k)$ have the following general form in Fourier space:

$$C_{ij}^{sym}(\tau) = \sum_f (x_{i,R}(f)x_{j,R}(f) + x_{i,I}(f)x_{j,I}(f)) \times \cos(2\pi f\tau) \quad (4)$$

where $x_{i,R}(f)$ and $x_{i,I}(f)$ are the real and imaginary part of the complex valued spectrum of $x_i(t)$. The expression in (4) is equivalent to a correlation between a spectrum of one signal filtered with $\cos(2\pi f\tau)$ and the unfiltered spectrum of a second signal. The frequency response of the filter can be seen as a frequency comb due to the periodicity of the cosine. Then, the delayed covariance matrices can be viewed as the correlation of spectra from different measurement channels weighted by a frequency comb, which favors harmonic spectra. This means that TDD can separate sources only if their spectra are different [13], [23]. This suits our experimental situation as we expect a periodic response from the brain at 3 Hz due to the periodic electrical stimulation (see Section II-C) and a different spectrum for noise signals such as, e.g., the heartbeat with a frequency around 1 Hz or power line noise at 50 Hz. All of the three mentioned signals contain harmonics of their respective base frequency, leading to comb-shaped spectra differing in the distance between individual peaks. For the comb-shaped filter function $\cos(2\pi f\tau)$, a frequency resolution f_{res} can be defined as the distance between two adjacent maxima of the cosine, which is $f_{\text{res}} = 1/\tau$. To achieve a certain frequency resolution, the necessary τ can be estimated using this simple rule.

B. Projection

To suppress or enhance certain field patterns in a multidimensional signal vector space, the signal space projection (SSP) was introduced in [24] and [25]. SSP is motivated by the observation

that brain signals and noise signals have very different field patterns, which means that they can be almost orthogonal toward each other in the signal space. In the SSP, a set of base vectors \mathbf{b}_i is split into two groups, which are denoted as parallel and orthogonal (\parallel , \perp). Then, projection operators \mathbf{P}_{\parallel} and \mathbf{P}_{\perp} are determined, which separate the signal into orthogonal subspaces: $\mathbf{x}_{\parallel}(t) = \mathbf{P}_{\parallel}\mathbf{x}(t)$ and $\mathbf{x}_{\perp}(t) = \mathbf{P}_{\perp}\mathbf{x}(t)$.

A matrix \mathbf{K} is formed using the $\{\mathbf{b}_i\}_{\parallel}$ -patterns as column vectors, and its singular value decomposition is calculated: $\mathbf{K} = \mathbf{U}\mathbf{\Lambda}\mathbf{V}^T$. The columns of \mathbf{U} form an orthonormal basis for the column space of \mathbf{K} , and the operators read

$$\mathbf{P}_{\parallel} = \mathbf{U}\mathbf{U}^T, \quad \mathbf{P}_{\perp} = \mathbf{I} - \mathbf{P}_{\parallel}. \quad (5)$$

In Section V-B, only a 1-D SSP is used as the $\{\mathbf{b}_i\}_{\parallel}$ group consists of a single vector, which is chosen from averaged data. The application of a 1-D \mathbf{P}_{\parallel} operator to the measured data $\mathbf{x}(t)$ is similar to the scalar product between the data vector and a second time-independent vector, where only the normalization is different in the SSP, preserving the signal magnitude of the resulting 1-D time series.

C. SEF N20m Measurements

In five healthy volunteers, the somatosensory MEG was recorded using a planar system described in [26]. It consists of 49 axial superconducting quantum interference device gradiometers arranged on a plane in a hexagonal grid with the gradiometer orientation nearly perpendicular to the plane. The planar system does not cover the whole head, but it is ideally suited to measure over a known anatomical location in close proximity to the head, and large MEG signal amplitudes can be obtained.

An electrical pulse of 100- μ s duration was applied to the medianus nerve with a strength of 5–10 mA, which is well above the motor threshold. The stimulation was on the right side with a frequency of 3 Hz. The MEG system was positioned with its central sensor over the somatosensory cortex contralateral to the stimulation (position C3 in the 10–20 system). The measurement of 4000 s was split into four blocks of 1000-s duration each. The data were sampled at 2 kHz after analog filtering with a bandpass of 0.1 to 1 kHz. We display the data from one subject consistently through all stages of analysis, as similar results were obtained for the other subjects. Data obtained using a whole head MEG system were found to be noisier and to appear less stationary. This is possibly due to a larger distance between cortex and sensors and a higher sensor noise level in the whole head system compared to the planar system. The whole head data will not be discussed here.

D. Application of TDD

Before applying the TDD algorithm, each individual channel of the multichannel raw data set was digitally bandpass filtered using two different passbands: i) A filter with a passband of 2 to 500 Hz and -60 -dB damping points at 1 Hz and 1 kHz was used to reduce the influence of the cardiac signal with a dominant frequency around 1 Hz and to reduce noise above 500 Hz. These data are denoted by WB (= wideband). ii) To reduce the influence of the 50-Hz line noise, which is the strongest signal in the

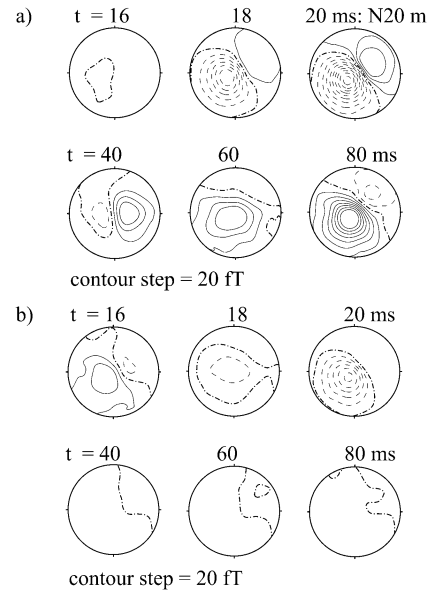


Fig. 1. (a) Maps from the averaged WB data measured during electrical stimulation at the medianus nerve showing at around 20 ms a dipolar pattern known as the N20m, and different dipolar structures appear at later times. (b) Average of the HP data. The dipolar structure at 20 ms is fairly similar to the WB data shown in (a), and the later activity is no longer present in (b).

TDD decomposition of the WB data, and to suppress commonly occurring 10 and 20 Hz brain signals (α , β , or μ oscillations), a second filter was applied. It had a passband of 55 to 500 Hz and -60 -dB damping points at 50 Hz and 1 kHz. These data will be denoted by HP (= highpass).

As time-delayed covariance matrices, a set of 500 matrices with $\tau_i = \{4, 8, 12, \dots, 2000\}$ ms was chosen empirically in the TDD calculation as there is no general rule for the choice of the set $\{\tau_i\}$. For the the largest τ_i , the corresponding frequency resolution introduced in Section II-A is $f_{\text{res}} = 1/2000$ ms = 0.5 Hz. This should be sufficient to distinguish harmonic spectra with a 1-Hz peak distance due to the cardiac activity from spectra with a 3-Hz peak distance due to the stimulation. Increasing the resolution further did not change the results.

A full recorded dataset consists of about 8×10^6 sampling points for each of 49 channels of the MEG system. To reduce the computing time, the TDD components were calculated using the data from the second measurement block only. A dimension reduction, e.g., using PCA, to achieve a further computing time reduction was abandoned as inferior results were obtained. With as little as 10 s of data, a useful TDD decomposition results; nevertheless, the 1000 s of data used yield a statistically better founded estimate.

III. AVERAGED WB AND HP DATA

The conventional analysis for an SEF measurement is given in Fig. 1, which shows maps from the average over 3000 epochs for the WB data in (a) and for the HP data in (b). A 5-ms baseline starting at 5 ms after the stimulus was subtracted. This baseline window is neither influenced by the stimulus artifact nor by early Thalamic activity [27]. Starting at 18 ms, activity is seen in (a), reaching its first maximum at 20 ms: the N20m. The map shows the well-known dipolar structure of the N20m, which can

be attributed to a point-like current source in the cortex [28], [29]. The distance between the field maxima is 8 cm (diameter of planar sensor array = 20 cm), and a source depth of about 2 cm below the skull can be estimated [29]. Later activity at 40, 60, and 80 ms shows maps that are different from the N20m.

The average over the HP data is shown in Fig. 1(b). The map at 20 ms is similar to the map obtained from the WB data in (a). The activity visible between 40 to 80 ms in the WB data in (a) is no longer present in the HP data in (b). This later activity belongs apparently to signal components below 55 Hz.

IV. RESULTS FOR WB DATA

A. Selected WB-TDD Components

Three TDD components calculated from the WB data are shown in Fig. 2, which are attributed to the medianus stimulation due to their spectra and their field map, as will be explained below. In this figure, each component is represented by its field map (left), an 8-s section of its time series (bottom right), and the spectrum of the full time series of 1000 s used in the TDD calculation (top right). The spectrum of component *SEF1wb* is shown in two parts for ease of interpretation. The scaling of the time series in units of femto Teslas (fT) was obtained after rescaling the maximum of the field map to one, i.e., the time series corresponds to the signal in the strongest sensor with respect to the field map.

The spectrum of *SEF1wb* has peaks starting at 3 Hz, the stimulation frequency, and nearly every harmonic of 3 Hz up to 200 Hz. The multitude of higher harmonics in the spectrum of *SEF1wb* implies that this component has very narrow peaks in the time domain, as will be discussed in Section V. These higher harmonics are not due to the stimulus artifact at 0 ms, which is a spike in the measured data due to the electrical stimulation pulse at the wrist. It is isolated by TDD into a separate stimulus artifact component, which is given in Fig. 5 as *STIMhp* for the HP data. The spectrum of *STIMhp* in Fig. 5 shows the 3-Hz harmonics without decreasing peak amplitude up to 300 Hz, and further peaks exist beyond the displayed range.

The structure of the dipolar map of *SEF1wb* in Fig. 2 clearly indicates a cortical source (cf. Section III). The maps of component *SEF2wb* and *SEF3wb* suggest that they represent brain activity as well. Their spectra contain a peak at 3 Hz on a broad background, and therefore, they are attributed to the medianus stimulation as well. These components seem to represent stimulus-related brain activity from a different location compared to *SEF1wb*.

The map of component *SEF1wb* is evidently similar to the averaged WB data at 18 and 20 ms in Fig. 1(a). To have a quantitative measure for the similarity of two patterns in the signal vector space an angle α can be calculated from $\cos \alpha = \mathbf{ab}/(|\mathbf{a}||\mathbf{b}|)$ [24], [30], where \mathbf{a} is the TDD base vector *SEF1wb*, and \mathbf{b} is the averaged WB data vector at 20 ms, which is shown as a map in Fig. 1(a). The resulting value $\alpha = 12^\circ$ shows the high degree of similarity.

Despite the results shown, other TDD components could be attributed to power line noise and the cardiac artifact discussed in [19].

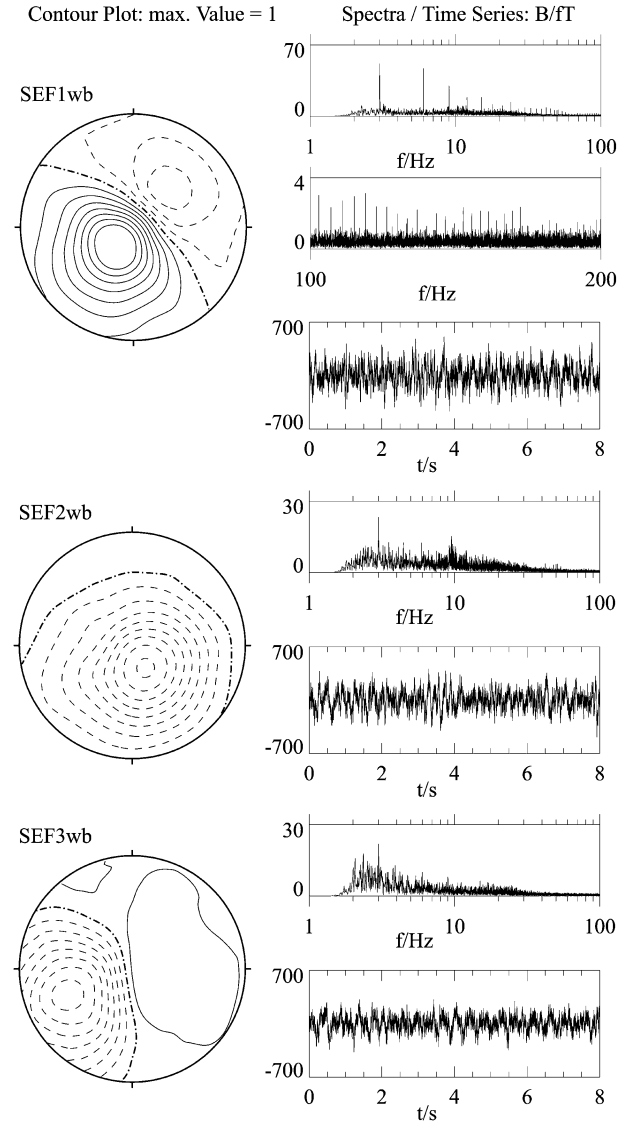


Fig. 2. Selected TDD components calculated from the raw WB data, which are attributed to the medianus stimulation. Each component pattern (field map, left) is shown together with a section of its time series (bottom right) and the power spectrum (top right) of the time series (the spectrum of *SEF1wb* is given in two parts). Component *SEF1wb* is clearly related to the stimulation as its map is similar to the N20m in Fig. 1(a), and its spectrum contains a harmonic series of peaks starting at 3 Hz.

B. Single Trial Plots

The single trial (ST) plot introduced and applied in [2], [17], [18], and [31] is a tool to visualize the common behavior in repetitive signals. Multiple sections of a time series are displayed as stacked grey shaded scan lines with the function value coded by the grey shade. The sections of the time series are aligned at a set of markers, which are the time points of the medianus stimulation in the present case. The abscissa of the plots is the time relative to the marker, and the ordinate counts the displayed sections of the time series. No smoothing across adjacent lines, i.e., along the ordinate axis, was performed for the ST plots.

The ST plots and averages for TDD components *SEF1wb* to *SEF3wb* are shown in Fig. 3. The upper panels show the response to 300 consecutive stimulations within the first measure-

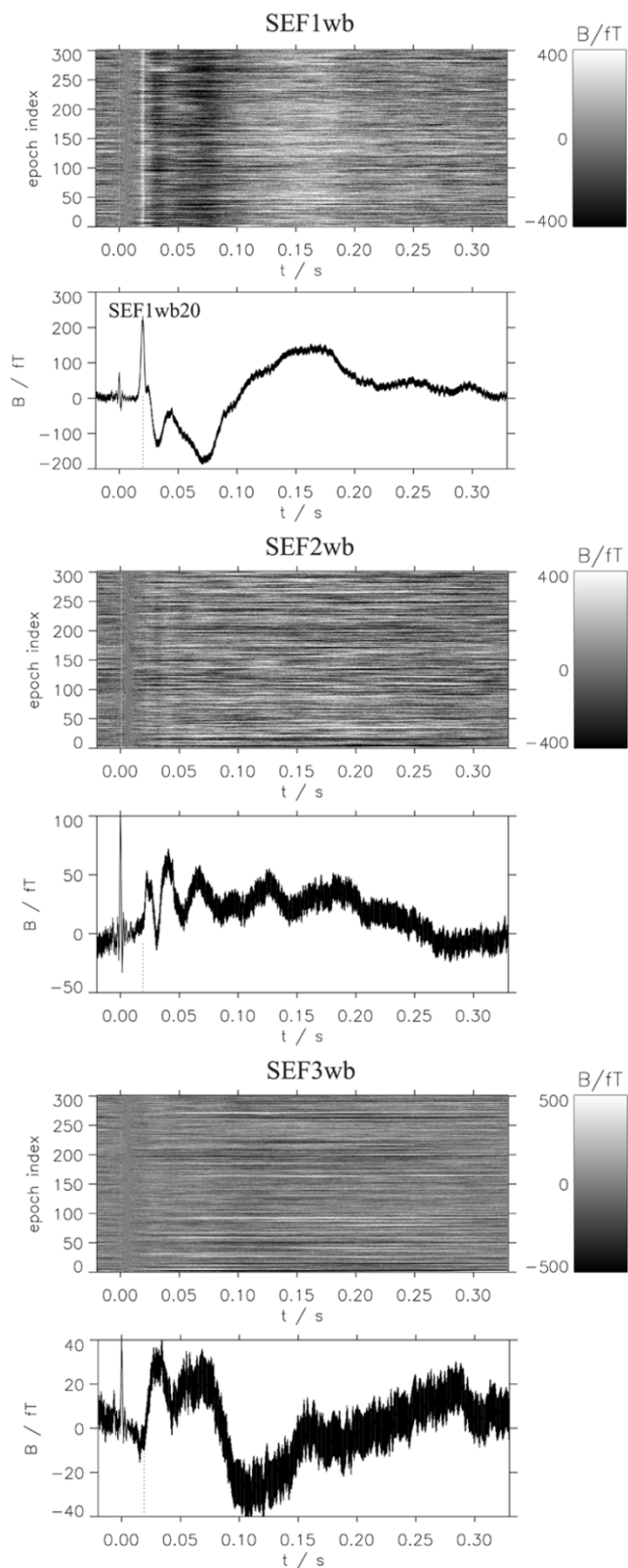


Fig. 3. ST plots and averages of components $SEF1wb$ – $SEF3wb$ shown in Fig. 2. The upper panels show the ST plots of 300 consecutive individual responses to the medianus stimulation. The lower panels are the averages over the epochs in the upper panels, and the width of the trace gives the SEM. Note the different scales. A strong response at 20 ms is observed for $SEF1wb$ in the ST plot and the average.

ment block. The coding between grey shade and field value is given by the vertical bar on the right. The lower panels show the

average over the epochs in the upper panel with up to 10% of outlying epochs with amplitudes larger than 850 fT rejected for the average. The baseline was calculated in the window used for the averaged data (5–10 ms after the stimulus). This leads to the reduced variance of the grey shades along the ordinate in the ST plots between 5 and 10 ms as zero time corresponds to the electrical stimulus. The line width of the average in the lower panel is the SEM of the individual values in the ST plot (outliers excluded).

The ST plot for $SEF1wb$ shows a thin vertical line at 20 ms, leading to a narrow peak in the average indicated by the dotted vertical line. This response, labeled $SEF1wb20$, is, in the TDD analysis, the equivalent of the N20m of the conventional average. Later and much broader responses can be seen both in the ST plot and the average at 30, 70, and 170 ms.

In contrast to that, $SEF2wb$ shows no activity at 20 ms, as can be seen best in the average, where the dotted vertical line is plotted again at 20 ms. This component is related to the stimulus artifact at 0 ms and activity at 30 ms. Component $SEF3wb$ represents a slow up and down sequence between 20 and 250 ms and is clearly stimulus related. The average amplitude of $SEF2wb$ and $SEF3wb$ is only a fraction of the amplitude of $SEF1wb$ (note the adjusted scales for the averages only). Inspection reveals that the absolute SEM values of the three components displayed are in the range of 6–10 fT, which suggests a similar variability for all components. Calculating the kurtosis for each time instance gave consistently positive kurtosis values for $SEF2wb$ and $SEF3wb$, i.e., their amplitude distribution has non-Gaussian wings. The difference between a Gaussian and non-Gaussian distribution leads to the clear response picture in the ST plot for $SEF1wb$ and the rather blurred images for $SEF2wb$ and $SEF3wb$.

The spectra of components $SEF2wb$ and $SEF3wb$ in Fig. 2 show a peak at 3 Hz, which is not surprising as the averages of both components in Fig. 3 contain prominent slow stimulus-related activity. The multitude of harmonics of 3 Hz in the spectrum of $SEF1wb$ is directly reflected in the small width of the $SEF1wb20$ peak in Fig. 3.

The ST plots and averages in Fig. 3 show that several TDD components carry stimulus-related activity, i.e., at least a three-dimensional (3-D) stimulus related signal space was found. This is in agreement with [32], where several cortical areas were found, contributing to the typical measured sequence of N20m, P35m, P60m, and later responses.

C. TDD Component Trend Analysis

In Fig. 3, only 300 of the 12 000 recorded epochs are displayed, and the physiologically interesting question arises whether the responses observed are stable over the full set of epochs. As an example, a trend analysis is shown in Fig. 4 for two groups of 500 epochs from component $SEF1wb$ chosen from the beginning and the end of the experiment (note the reduced time axis compared to Fig. 3). The averages over the two ST plots in Fig. 4(a) are shown in (b) (solid line: epoch 1000–1500, dotted line: epoch 10500–11 000), together with their SEM. The $SEF1wb20$ response introduced in the previous section is almost identical in the averages in Fig. 4(b) for both groups of epochs, but a large difference is observed between

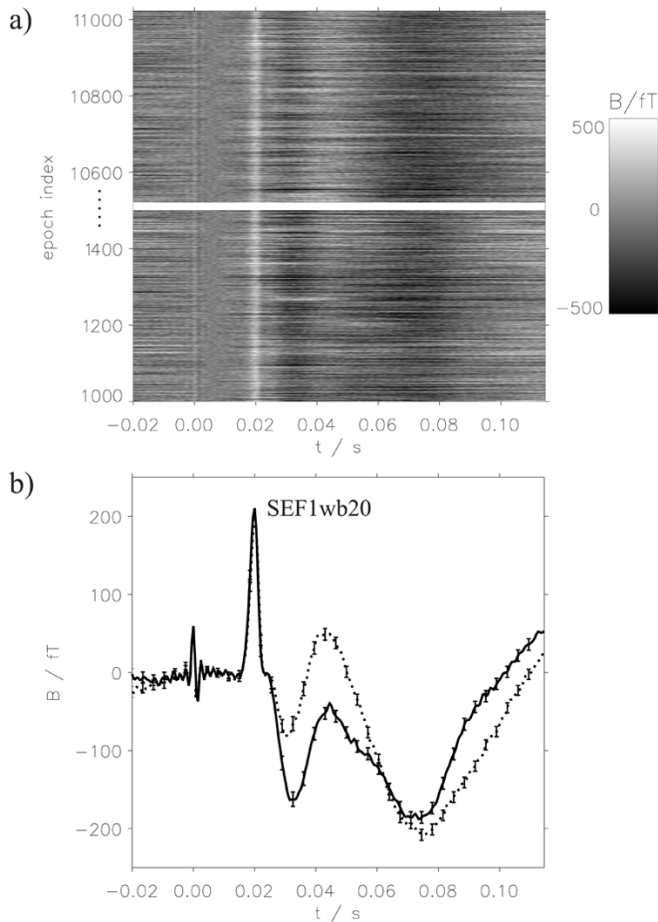


Fig. 4. Trend analysis for component *SEF1wb*. (a) ST plots of two groups of 500 individual stimulation epochs chosen as indicated. (b) Respective averages (solid line: epoch 1000–1500, dotted line: epoch 10500–11000) together with their SEM (small error bars).

30 and 60 ms for the two groups. This difference is clearly visible in the ST plots in Fig. 4(a) and the averages in (b), and it is highly significant, as can be easily estimated using a standard t-test: At $t = 45$ ms, the difference of the averages in (b) is ≈ 100 fT, SEM ≈ 10 fT, and number of epochs = 300, then a significance of better than 99.99% results. In contrast to that, the difference of ≈ 10 fT in the *SEF1wb20* response of both groups is not even close to significance. Changes in the attentional focus or habituation effects might explain the observed effect between 30 and 60 ms. Note that the calculation of a significance level for a difference between subaverages is not possible using the standard method of averaging.

V. RESULTS FOR HP DATA

A. Selected HP-TDD Components

In Fig. 5, two selected TDD components calculated from the HP data are shown. In the time series (lower right trace) of *SEF1hp*, evenly spaced peaks are visible above the noise level. The spacing is about 330 ms, as can be seen best between the second 2 and 3. These peaks are interpreted as the individual responses at 20 ms after the stimulation, as will be discussed in Section V-B. The angle α defined in Section IV-A between the map of *SEF1hp* and the map of the averaged signal at 20 ms in

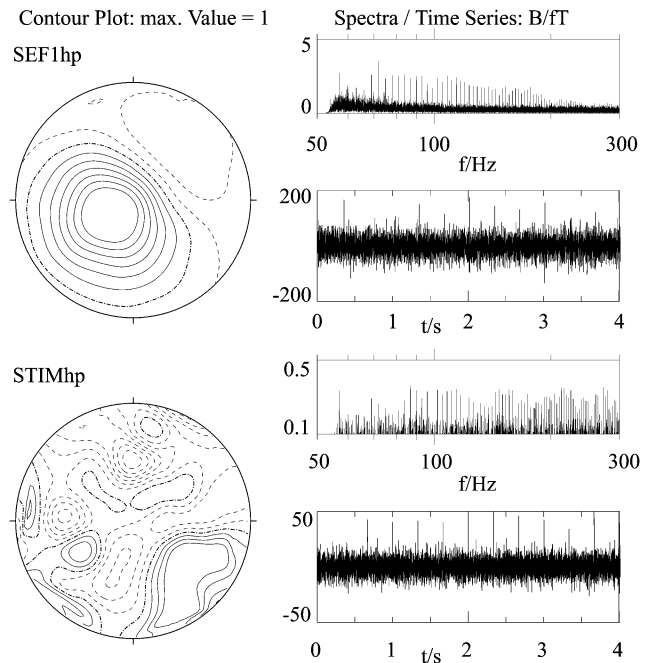


Fig. 5. Selected TDD components calculated from the HP raw data. The layout of the figure is the same as in Fig. 2. Component *SEF1hp* is evidently related to the stimulation as its map is similar to the map at 20 ms in Fig. 1(b), and its spectrum contains the harmonics of the 3 Hz stimulation frequency. The stimulus artifact leads to component *STIMhp* exhibiting harmonics of 3 Hz in its spectrum, which extend beyond the displayed range.

Fig. 1(b) is $\alpha = 10^\circ$. This supports additionally that component *SEF1hp* is related to the medianus stimulation. The dipolar field pattern of *SEF1hp* again suggests a cortical origin.

As already discussed in Section IV-A, the component *STIMhp* in Fig. 5 is due to the stimulus artifact. Close inspection reveals that it has peaks in its time series just before the response peaks in the time series of *SEF1hp*. This delay can be seen at $t = 2$ s in Fig. 5. The map of *STIMhp* is very irregular, which is typical of a technical artifact signal.

B. Single-Response Statistics

The WB data discussed in Section IV have already shown that at 20 ms, a clear stimulus-induced response can be observed in the TDD components without averaging (see Fig. 3). The single trial response is even more stable in the HP data, as can be seen from the ST plots over 100 consecutive epochs in Fig. 6, which gives a comparison between the results from conventional methods of signal processing in Fig. 6(a) to the TDD result in (b).

To obtain the result in Fig. 6(a), the HP data were notch filtered at the harmonics of 50 Hz, i.e., 100, 150, ... Hz, followed by a P_{\parallel} projection, as given in (5), Section II-B. To isolate the response at 20 ms, it was a natural choice to use only the average map at 20 ms of the HP data in Fig. 1(b) as the projection pattern for P_{\parallel} . The ST plot for the time series resulting from P_{\parallel} is shown in the upper panel in Fig. 6(a). The stimulus artifact is observed at 0 ms and a clear response at 20 ms, which is labeled PRhp20. The average over the set of individual responses is given in the lower panel of Fig. 6(a), together with the SEM (error bars = line width). The SEM for the average of component *SEF1hp* in Fig. 6(b) is almost too small to display,

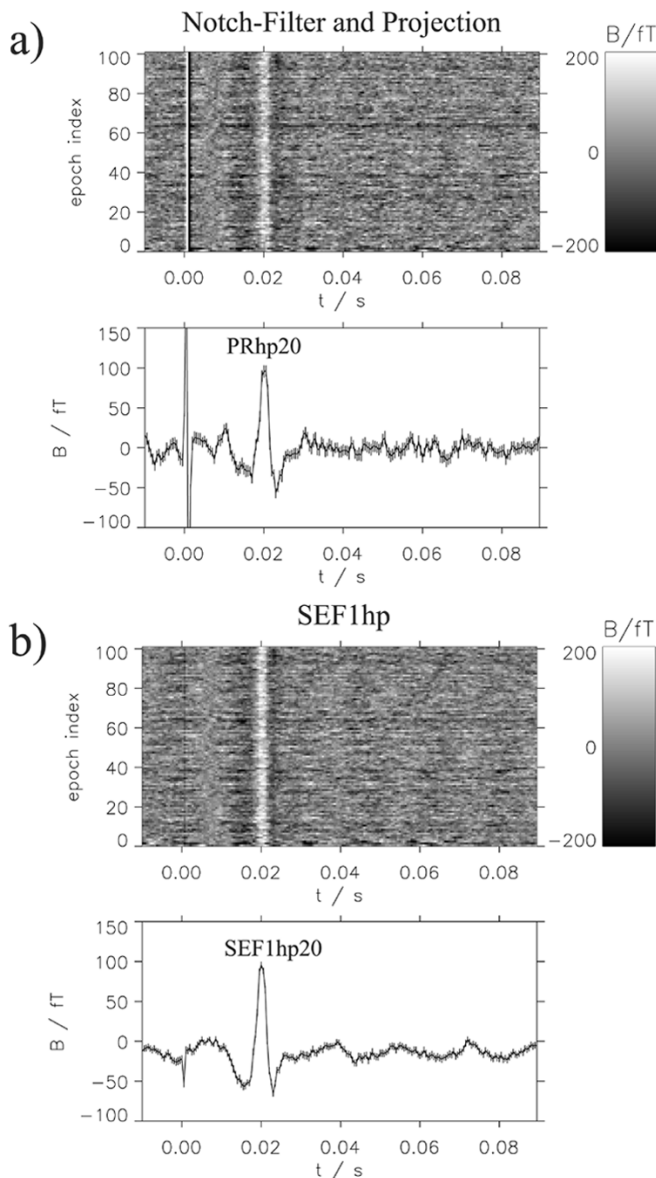


Fig. 6. (a) ST plot and average of a time series obtained by projection and notch filtering (s. text). (b) ST plot and average of component *SEF1hp*. The ST plots and the averages show a sharp response at 20 ms, which are labeled *PRhp20* and *SEF1hp20*, respectively. The response at 20 ms is clearer in the ST plot for *SEF1hp* in (b), corresponding to the lower SEM in the average (error bars = line width).

and the SEM is clearly smaller than in the projection. The stimulus artifact at 0 ms is nearly invisible in the ST plot of the TDD component in Fig. 6(b), showing the superior signal separation capabilities of the TDD-ICA compared with the projection.

The responses at 16 ms in Fig. 6(a) and (b) can be either artifactual filter rebound or might be due to early signals from the cerebellum [27]. Only signals at later times are discussed here, and with the knowledge of the WB data, the *PRhp20* and *SEF1hp20* responses can be safely attributed to a physiological process.

The ST plot of *SEF1hp20* in Fig. 6(b) seems to show a positive response in each epoch at 20 ms. To investigate this quantitatively, the amplitude distributions of the *PRhp20* and *SEF1hp20* responses were calculated for all 12 000 stimulations of the experiment. Fig. 7 shows these distributions for

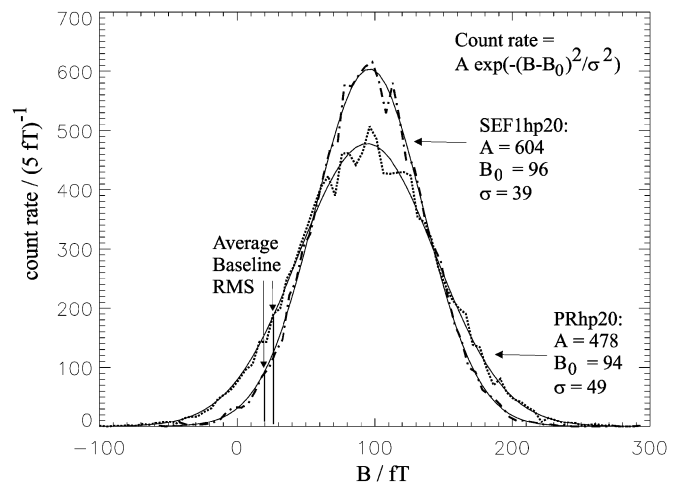


Fig. 7. Amplitude distributions of the *PRhp20* (dotted line) and *SEF1hp20* (dash dotted line) responses for all 12 000 stimulations measured. The distribution is clearly narrower for the *SEF1hp20* response, as quantified by the fitted Gaussian functions (solid lines). The sum of detectable responses is defined by the area under the distribution for fields above the average baseline RMS. With this measure, 97% of the responses are detectable for *SEF1hp20* and 91% for *PRhp20*.

the sample point at 20 ms using a bin width of 5 ft. The distribution for the *SEF1hp20* response (dash dotted line) is clearly narrower compared with the distribution for the *PRhp20* response (dotted line). The distributions can be approximated by a Gaussian, as can be seen from the solid lines, which are least-squares fits, resulting in the parameters given in the figure. As the data at 20 ms in Fig. 6 are contained in the distributions in Fig. 7, the means of the distributions are similar to the averages at 20 ms in Fig. 6.

To give a quantitative assessment, whether each individual stimulation leads to a response, a threshold was defined as the average RMS value of the projection and *SEF1hp* time series in the baseline interval between 5 and 10 ms. These thresholds are given in Fig. 7 by the vertical lines. All responses below this threshold, i.e., to the left of the respective vertical lines in Fig. 7, will be defined as nondetectable. The number of nondetectable responses is found to be 1067 for the *PRhp20* and only 317 for the *SEF1hp20* response, which are about 8.9% and 2.6%, respectively, of the total number of stimulations. This shows that 97% of the stimulations lead to a response above base line noise level at 20 ms in the TDD component *SEF1hp* and 91% using the conventional projection method.

VI. CONCLUSION

Applying the TDD algorithm to MEG data measured under electrical stimulation of the medianus nerve, we were able to isolate individual signal peaks occurring typically 20 ms after the stimulation. This can be seen in the ST plots in Figs. 3 and 4 and best in Fig. 6. The typical field patterns from the conventionally averaged data in Fig. 1 are very similar to the TDD components in Figs. 2 and 5, as the angle between TDD component and average pattern is $\alpha = 12^\circ$ for the WB and $\alpha = 10^\circ$ for the HP data. Therefore, it can be concluded that the TDD components containing the individual signal peaks and the average reflect the same underlying brain responses. The variation

in the ST plots in Fig. 3, together with the SEM of the respective averages, showed that the SEM alone is not a good quantity to characterize the statistical properties of the TDD components.

The trend analysis in Fig. 4 can be compared with the results for similar experimental data obtained using a maximum likelihood estimator in [11] and a single channel ST plot in [31]. A continuous trend analysis is performed in [11] for early responses between 20 and 35 ms and later responses starting at 30 ms. The early responses show trends in both directions for the nine subjects studied, and the later responses show a decrease. The result in Fig. 4 differentiates between 20 and 30 ms with no change at 20 ms and a decrease in strength at 30 ms, which agrees with the result in [11]. The similarity between the results in [11] and the present work shows the validity of both approaches. In [31], a decrease of activity is found between 50 and 100 ms, although no statistical analysis is presented. We see a significant decrease at even earlier times in Fig. 4, which is probably due to the better signal quality of the TDD component and is evident by comparing our SEF1wb20 response with the response in the single-channel ST plot at 20 ms in [31].

Early somatosensory response peaks due to tactile stimuli were detected using TDD in [17]. A peak width of 20–40 ms was found, and the peak latency of the single trials varied within 50 ms. The responses due to electrical stimulation found in our work are rather different as they have a width < 5 at 20 ms and show an onset variation of only a few milliseconds, as can be estimated from Figs. 4 and 6.

The ST plots in Fig. 6 and the statistical analysis in Fig. 7 show that for the subject displayed here, 97% of the stimulations lead to a measurable cortical response at 20 ms. This result is not trivial, as only the application of the highpass filtering and TDD-ICA allowed us to reach such a high percentage of measurable responses. Our findings are experimental support for the postulate that variability is minimal at the early stages of cortical sensory processing [33]. The question requires further study as other works using single trial methods find more variability in the early stages of somatosensory [10], [11] and visual processing [34], although again, small variability is found for auditory processing [35].

ACKNOWLEDGMENT

Help with the measurements by G. Nolte and the usage of a software package developed by G. Wübbeler are gratefully acknowledged.

REFERENCES

- [1] A. Hyvärinen, J. Karhunen, and E. Oja, *Independent Component Analysis*. New York: Wiley, 2001.
- [2] T. P. Jung, S. Makeig, M. J. McKeown, A. J. Bell, T. W. Lee, and T. Sejnowski, "Imaging brain dynamics using independent component analysis," *Proc. IEEE*, vol. 89, no. 7, pp. 1107–1122, Jul. 2001.
- [3] J. V. Stone, "Independent component analysis: An introduction," *TRENDS Cogn. Sci.*, vol. 6, pp. 59–64, 2002.
- [4] M. J. McKeown, "Detection of consistently task-related activations in fMRI data with hybrid independent component analysis," *Neuroimage*, vol. 11, pp. 24–35, 2000.
- [5] F. Bijma, J. C. de Munck, H. M. Huizenga, and R. M. Heethaar, "A mathematical approach to the temporal stationarity of background noise in MEG/EEG measurements," *Neuroimage*, vol. 20, pp. 233–243, 2003.
- [6] T. H. Sander, M. Burghoff, A. Lueschow, G. Curio, and L. Trahms *et al.*, "Unsupervised identification of spontaneous magnetoencephalographic alpha activity by independent component analysis," in *Proc. 13th Int. Conf. Biomagnetism*, H. Nowak *et al.*, Eds., 2002, pp. 991–993.
- [7] J. Tiihonen, R. Hari, and M. Hämäläinen, "Early deflections of cerebral magnetic responses to median nerve stimulation," *Elec. Clin. Neuro.*, vol. 74, pp. 290–296, 1989.
- [8] R. Hari and N. Forss, "Magnetoencephalography in the study of human somatosensory processing," *Phil. Trans. R. Soc. Lond. B*, vol. 354, pp. 1145–1154, 1999.
- [9] R. Kakigi, M. Hoshiyama, M. Shimojo, D. Naka, H. Yamasaki, S. Watanabe, J. Xiang, K. Maeda, K. Lam, K. Itomi, and A. Nakamura, "The somatosensory evoked magnetic fields," *Prog. Neurobiol.*, vol. 61, pp. 495–523, 2000.
- [10] A. A. Ioannides, G. K. Kostopoulos, N. A. Laskaris, L. Liu, T. Shibata, M. Schellens, V. Poghosyan, and A. Khurshudyan, "Timing and connectivity in the human somatosensory cortex from single trial mass electrical activity," *Human Brain Mapp.*, vol. 15, pp. 231–246, 2002.
- [11] J. C. de Munck, F. Bijma, P. Gaura, C. A. Sieluzycycki, M. I. Branco, and R. M. Heethaar, "A maximum-likelihood estimator for trial-to-trial variations in noisy MEG/EEG data sets," *IEEE Trans. Biomed. Eng.*, vol. 51, no. 12, pp. 2123–2128, Dec. 2004.
- [12] L. Molgedey and H. G. Schuster, "Separation of a mixture of independent signals using time delayed correlations," *Phys. Rev. Lett.*, vol. 72, pp. 3634–3637, 1994.
- [13] A. Belouchrani, K. Abed-Meraim, J.-F. Cardoso, and E. Moulines, "A blind source separation technique using second-order statistics," *IEEE Trans. Signal Process.*, vol. 45, no. 2, pp. 434–444, Feb. 1997.
- [14] A. Ziehe and K.-R. Müller *et al.*, "TDSEP—An efficient algorithm for blind separation using time structure," in *Proc. 8th ICANN*, L. Niklasson *et al.*, Eds., 1998, pp. 675–680.
- [15] A. Ziehe, K.-R. Müller, G. Nolte, B.-M. Mackert, and G. Curio, "Artifact reduction in magnetoneurography based on time-delayed second order correlations," *IEEE Trans. Biomed. Eng.*, vol. 47, no. 1, pp. 75–87, Jan. 2000.
- [16] G. Wübbeler, A. Ziehe, B.-M. Mackert, K.-R. Müller, L. Trahms, and G. Curio, "Independent component analysis of noninvasively recorded cortical magnetic DC-fields in humans," *IEEE Trans. Biomed. Eng.*, vol. 47, no. 5, pp. 594–599, May 2000.
- [17] A. C. Tang, B. A. Pearlmutter, N. A. Malaszenko, and D. B. Phung, "Independent components of magnetoencephalography: Single-trial response onset times," *Neuroimage*, vol. 17, pp. 1773–1789, 2002.
- [18] A. C. Tang, B. A. Pearlmutter, N. A. Malaszenko, D. B. Phung, and B. C. Reeb, "Independent components of magnetoencephalography: Localization," *Neural Comput.*, vol. 14, pp. 1827–1858, 2002.
- [19] T. H. Sander, G. Wübbeler, A. Lueschow, G. Curio, and L. Trahms, "Cardiac artifact subspace identification and elimination in cognitive MEG data using time-delayed decorrelation," *IEEE Trans. Biomed. Eng.*, vol. 49, no. 4, pp. 345–354, Apr. 2002.
- [20] M. Kawakatsu, H. Ishibashi, K. Kobayashi, Y. Uchikawa, and M. Kotani *et al.*, "The discrimination index of the evoked field components in ICA," in *Proc. 13th Int. Conf. Biomagnetism*, H. Nowak *et al.*, Eds., 2002, pp. 1021–1023.
- [21] K. Kishida, K. Kato, K. Shinosaki, and S. Ukai, "Blind identification of SEF dynamics from MEG data by using decorrelation method of ICA," in *Proc. 4th Int. Symp. ICA BSS*, 2003, pp. 185–190.
- [22] A. C. Tang, M. T. Sutherland, and C. J. McKinney, "Validation of SOBI components from high-density EEG," *Neuroimage*, vol. 25, pp. 539–553, 2002.
- [23] A. Ziehe, G. Nolte, G. Curio, and K.-R. Müller, "OFI: Optimal filtering algorithms for source separation," in *Proc. 2nd Int. Workshop ICA BSS*, P. Pajunen and J. Karhunen, Eds., Helsinki, Finland, 2000, pp. 127–132.
- [24] M. Huotilainen, R. J. Ilmoniemi, H. Tiitinen, J. Lavikainen, K. Alho, M. Kajola, and R. Näätänen *et al.*, "The projection method in removing eye-blink artifacts from multichannel MEG measurements," in *Biomagnetism: Fundamental Research and Clinical Applications*, C. Baumgartner *et al.*, Eds. New York: Elsevier Sci. IOS, 1995, pp. 363–367.
- [25] M. A. Uusitalo and R. J. Ilmoniemi, "Signal-space projection method for separating MEG or EEG into components," *Med. Biol. Eng. Comput.*, vol. 35, pp. 135–140, 1997.
- [26] D. Drung, "The PTB 83-SQUID-system for biomagnetic applications in a clinic," *IEEE Trans. Appl. Supercond.*, vol. 5, no. 2, pp. 2112–2117, Jun. 1995.
- [27] C. D. Tesche and J. Karhu, "Somatosensory evoked magnetic fields arising from sources in the human cerebellum," *Brain Res.*, vol. 744, pp. 23–31, 1997.

- [28] G. Curio, B.-M. Mackert, M. Burghoff, J. Neumann, G. Nolte, M. Scherg, and P. Marx, "Somatotopic source arrangement of 600 Hz oscillatory magnetic fields at the human primary somatosensory hand cortex," *Neurosci. Lett.*, vol. 234, pp. 131–134, 1997.
- [29] S. J. Williamson and L. Kaufmann, "Analysis of neuromagnetic signals," in *Handbook of Electroencephalography and Clinical Neurophysiology*, A. S. Gevins and A. Remond, Eds. Amsterdam, The Netherlands: Elsevier, 1987, vol. 1, pp. 405–448.
- [30] G. Gratton, M. G. H. Coles, and E. Donchin, "A procedure for using multi-electrode information in the analysis of components of the event-related potential: Vector filter," *Psychophysiol.*, vol. 26, pp. 222–232, 1989.
- [31] V. V. Nikouline, H. Wikström, K. Linkenkaer-Hansen, M. Kesaäniemi, R. J. Ilmoniemi, and J. Huttunen, "Somatosensory evoked magnetic fields: Relation to pre-stimulus mu rhythm," *Clin. Neurophysiol.*, vol. 111, pp. 1227–1233, 2000.
- [32] V. Jousmäki and N. Forss, "Effects of stimulus intensity on signals from human somatosensory cortices," *Neuro Rep.*, vol. 9, pp. 3427–3431, 1998.
- [33] V. B. Mountcastle, *Perceptual Neuroscience: The Cerebral Cortex*. Cambridge, MA: Harvard Univ. Press, 1998.
- [34] N. A. Laskaris, L. C. Liu, and A. A. Ioannides, "Single-trial variability in early visual neuromagnetic responses: An explorative study based on the regional activation contributing to the N70m peak," *Human Brain Mapp.*, vol. 15, pp. 231–246, 2002.
- [35] A. Salajegheh, A. Link, C. Elster, M. Burghoff, T. Sander, L. Trahms, and D. Poeppel, "Systematic latency variation of the auditory evoked M100: From average to single-trial data," *Neuroimage*, vol. 23, pp. 288–295, 2004.



Tilmann H. Sander was born in Freiburg, Germany, in 1965. He received the physics diploma from the Swiss Federal Institute of Technology, Zürich, Switzerland, and the Ph.D. degree in experimental semiconductor physics from Imperial College, London, U.K., in 1992 and 1996, respectively.

Since 1998, he has been a Research Associate with the Laboratory for Bioelectricity and Biomagnetism, Physikalisch-Technische Bundesanstalt, Berlin, Germany. His research interests include biomagnetism, instrumentation, and data analysis.



Martin Burghoff was born in Apolda, Germany, in 1952. He received the M.Sc. degree in technical cybernetics from the Technical University of Wrocław, Wrocław, Poland, and the Dr. Techn. degree in technical engineering from the Technical University of Ilmenau, Ilmenau, Germany, in 1976 and 1992, respectively.

Currently, he is a Senior Researcher with the Laboratory of Bioelectricity and Biomagnetism, Physikalisch-Technische Bundesanstalt, Berlin, Germany. His main research interests include biomagnetism, magnetoneurography, magnetocardiography, and the inverse problem.

Gabriel Curio was born in Berlin, Germany. He graduated from the Berlin School of Medicine, received the M.D. degree, and completed the specialization in neurology and psychiatry, from Charité University Medicine Berlin, where he is currently an adjunct professor of neurology.

He is leading the Neurophysics Group, Department of Neurology, Charité Campus Benjamin Franklin, University of Medicine, Berlin. His main interest is the integration of the neurophysics of noninvasive electromagnetic brain monitoring with both basic and clinical neuroscience concepts. His recent research interests include spike-like activities in somatosensory-evoked brain responses, injury currents, magnetoneurography, speech-hearing interactions, and brain computer interfaces.



Lutz Trahms was educated in physics at the Technical University Aachen, Aachen, Germany, and later at Freie Universität Berlin, Berlin, Germany, from which he received the Ph.D. degree in 1982.

He held a Postdoctoral Position at Freie Universität Berlin, where he used NMR spectroscopy for biomembrane research. In 1986, he joined the Physikalisch-Technische Bundesanstalt, Berlin, where he has been head of the Laboratory for Bioelectricity and Biomagnetism since 1993. His current research interests are biosignal processing, the SQUID measurement technique, relaxation of magnetic nanoparticles, and broadband low field NMR.